Carbon 105 (2016) 401–407

Contents lists available at ScienceDirect

Carbon

journal homepage: www.elsevier.com/locate/carbon

Black diamond for solar energy conversion

Paolo Calvani [a, *], Alessandro Bellucci [a, b], Marco Girolami [a], Stefano Orlando [c], Veronica Valentini [a], Riccardo Polini [a, d], Daniele M. Trucchi [a, **]

[a] Istituto di Struttura della Materia (ISM), Unit of Montelibretti, Consiglio Nazionale delle Ricerche (CNR), Research Area of Rome 1, Via Salaria km 29.300, 00015 Monterotondo Scalo, Roma, Italy
[b] Dipartimento di Fisica, Università di Roma "Sapienza", Piazzale Aldo Moro 2, 00185 Roma, Italy
[c] Istituto di Struttura della Materia (ISM), Unit of Potenza, Consiglio Nazionale delle Ricerche (CNR), Zona Industriale, 85050 Tito Scalo, PZ, Italy
[d] Dipartimento di Scienze e Tecnologie Chimiche, Università di Roma "Tor Vergata", Via della Ricerca Scientifica 1, 00133 Roma, Italy

ARTICLE INFO

Article history:
Received 14 January 2016
Received in revised form
3 March 2016
Accepted 7 April 2016
Available online 20 April 2016

ABSTRACT

Black diamond is obtained by a controlled nanoscale periodic texturing of CVD diamond surface, able to drastically modify the interaction with solar radiation from optical transparency up to solar absorptance values even >90%. Surface texturing, performed by the use of an ultra-short pulse laser, is demonstrated to induce an intermediate band within the diamond bandgap supporting an efficient photoelectronic conversion of sub-bandgap photons (<5.5 eV). The intermediate band introduction results in an external quantum efficiency enhanced up to 800 nm wavelengths (and up two orders of magnitude larger than the starting transparent diamond film), without affecting the film transport capabilities. The optical and photoelectronic outstanding results open the path for future application of black diamond as a photon-enhanced thermionic emission cathode for solar concentrating systems, with advantages of excellent electronic properties combined with a potentially very low work function and high thermal stability.

1. Introduction

Diamond is an attractive material for the development of electronic devices owing to its outstanding electronic properties such as high carrier mobility, high breakdown electric field and high carrier saturation velocity [1]. Diamond has high resistance to radiation damage and low leakage currents, associated to its wide bandgap (E_G = 5.47 eV), so that it has been successfully exploited for the fabrication of ionizing radiation detectors [2–6]. Moreover, the low dielectric constant of 5.7 and the high thermal conductivity make diamond a suitable substrate for high power devices fabrication [7,8].

Diamond achieves negative electron affinity (NEA) conditions by hydrogen surface termination, meaning that electrons in the conduction band do not experience an energy barrier towards a vacuum escape, corresponding to a significant work function reduction. If diamond is also nitrogen- or phosphorous-doped, work function can be reduced to 1.7 eV or 0.6 eV, respectively. Under vacuum the C–H surface bond is stable up to 800 °C: diamond thermionic emitters were preliminary tested in conversion devices for solar concentrating systems [9,10].

Nowadays, considerable effort is dedicated to the development of high temperature photocathodes (Photon Enhanced Thermionic Emission – PETE devices [11]) for solar concentrating systems, that is a promising and efficient energy conversion mechanism. Nevertheless, this application needs low work function cathodes. The present approach, based on bandgap engineering of III–V semiconductors, natively characterized by high work function only reducible by toxic alkali metal-based coatings, reveals technological limitations owing to thermal instability both of the emitting coating and of the semiconductor lattice itself. These issues reduce sensibly the temperature operating range.

Conversely, the idea of using a low work function diamond for a PETE cathode clashes against its wide bandgap, that corresponds to an optical transparency. An engineering of diamond is mandatory to overcome this issue and attribute to it the desired functionalities. Authors already reported [12] on diamond plates irradiated with high-intensity femtosecond laser pulses, finding a significant absorption enhancement in visible and infrared range due to the

* Corresponding author.
** Corresponding author.
E-mail addresses: paolo.calvani@ism.cnr.it (P. Calvani), daniele.trucchi@ism.cnr.it (D.M. Trucchi).

http://dx.doi.org/10.1016/j.carbon.2016.04.017

formation of a surface periodic texturing. This absorption gives a characteristic black color to the initially transparent diamond samples: black diamond. Nevertheless, high absorptance in the solar spectrum is not sufficient for an efficient solar device: photocarriers have to be generated within the semiconductor and transported to the external circuit. In this paper the fabrication of black diamond and the optimization of its physical properties is extended to the demonstration of a significant photoelectronic generation with a sunlight excitation, that is the key-step for highly performing solar devices. Surface texturing by the controlled use of ultra-short laser pulses, avoiding the involvement of complicated lithographic steps and surface post-processing, represents a practical tool for a defect-engineering strategy on diamond. It is obtained by producing an intermediate band, namely introducing electronically active defects and related energy levels in diamond wide bandgap, able to electrically exploit the interaction with solar spectrum photons. This strategy is alternative to the standard bandgap engineering on III–V semiconductors, consisting on the optimization of the bandgap value with respect to the radiation to interact with. The control of the texturing characteristics (morphology, periodicity, depth, etc.) corresponds to the control of the energy position, density, and character of the introduced defect.

2. Experimental results

Samples used in this work are freestanding optical-grade (OG) polycrystalline CVD diamond discs (8 mm diameter, 0.5 mm thickness). Ultrashort-pulse (120 fs) laser beam, horizontally polarized and at a wavelength of 800 nm, is focused perpendicularly to the diamond surface in a high vacuum chamber ($<10^{-7}$ mbar) [12]. The pulse energy is kept constant at 3.6 mJ, for a power density of 2×10^{14} W cm^{-2} higher than the diamond ablation threshold (2×10^{12} W cm^{-2} [13,14]). The diamond target is moved along the two directions orthogonal to the laser axis with selectable speed to vary the impinging radiation dose D, defined as the energy of a single pulse multiplied by the number of pulses impinging the sample surface unit, from 2.5 to 12.5 kJ cm^{-2}. After the treatment, residual debris and graphitic-based contents are removed in a strongly oxidizing solution (H_2SO_4:$HClO_4$:HNO_3 in the 1:1:1 ratio, 15 min at boiling point). In this work, three nominally identical polycrystalline diamond samples are treated according to different doses and results are compared with those of the untreated one. Treatment parameters are summarized in Table 1.

Fig. 1a shows the untreated and black diamond samples after the wet etching process. The treated ones show a characteristic black color that qualitatively indicates a high absorption of visible light and justifies the name black diamond.

2.1. Morphology and structural characterization

Scanning Electron Microscopy (SEM) images of the diamond samples, obtained by field-emission gun SEM (FEG-SEM Leo Supra-35), are shown in Fig. 1b–e. The formation of surface periodic structures is evident for all the samples, perpendicularly oriented with respect to the laser beam polarization. For the lowest dose (D = 2.5 kJ cm^{-2}), structures with an irregular periodicity are formed (Fig. 1c), whereas, by increasing D to 5.0 kJ cm^{-2} (Fig. 1d), the treatment defines laser-induced periodic surface structures (LIPSS), already observed in literature [15], characterized by several micrometers long ripples of period $\lambda_r \cong 170$ nm, far shorter than the laser wavelength λ_l. The ripples depth, investigated by SEM in tilted configuration, has been found to be around 500 nm. The formation mechanism of these high-spatial-frequency LIPSS is debated in literature but it is typically related to the interaction of the laser pulse with the laser-induced plasma [15–19], producing ripples with periodicity equal to $\lambda_l/2n$, being n the refractive index of the target material. For OG diamond, $n = 2.41$ at 800 nm has been derived by optical characterization, in agreement with literature [20], so the resulting λ_r is 167 nm, confirmed by SEM characterization. Finally, the highest dose (12.5 kJ cm^{-2}) induces non-homogeneous ripples, characterized by sharp interruptions (Fig. 1e). This preliminary morphologic analysis highlights that a trade-off dose exists around 5.0 kJ cm^{-2}, where the formation of ordered periodic structures occurs.

After the development of the black diamond films, Raman spectroscopy was used to verify that the optical absorption enhancement was not related to non-diamond residuals (e.g. graphitic phases) and to analyze if bulk physical properties were affected by the treatment. Spectra were acquired at room temperature with an Ar^+ laser (514.5 nm), in back-scattering geometry, by using a Dilor XY triple spectrometer (1 cm^{-1} resolution) equipped with a liquid nitrogen cooled charge coupled device (CCD) detector and an adapted Olympus microscope arranged in confocal mode; the spot size was 2 μm. Spectra, obtained on 20 different points on the sample to provide a suitable statistics, were processed using the Thermo Grams Suite v9.2 software to determine line widths and intensities. Even if an excitation laser wavelength of 514.5 nm cannot disentangle surface from bulk contribution, useful indications about the material modification can be derived, since the treated region depth represents only 0.1% of the sample thickness. Spectra of investigated fs-laser treated CVD diamond samples are shown in Fig. 1f. Graphitic phases introduced by surface texturing are excluded by the absence of significantly increased broad peaks at 1380 and 1580 cm^{-1} compared to the pristine sample spectrum. Raman peak around 1332 cm^{-1}, typical of diamond [21], is sharp for all samples. The inset of Fig. 1f magnifies the features of diamond peaks, which position and Full Width Half Maxima (FWHM) at different treatment doses are summarized in Table 1. FWHM of Raman peaks is related to crystal quality in terms of amount of plastic deformation, and it is sensitive to structural parameters such as size, shape and distribution of grains [22,23]: the treated samples have a slightly broader peak than the untreated one, indicating a negligible introduction of disorder into the crystal structure. The upshift of diamond peak to higher wavenumbers, increasingly depending on treatment dose, could indicate the presence of a lattice compressive stress with respect to the untreated sample [24–28]. Nevertheless, such an upshift could be ascribed to a size effect of the structures that will be investigated in the future [29].

Table 1
Femtosecond laser treatment details for investigated samples.

Sample	Laser fluence [J cm^{-2}]	Treatment power density [W cm^{-2}]	Number of Fs-laser pulses	Dose D [kJ cm^{-2}]	Raman peak [cm^{-1}]	FWHM [cm^{-1}]
OG-1	–	–	–	–	1332.50 ± 0.03	3.05 ± 0.07
OG-2	20	2×10^{14}	7×10^5	2.5	1332.95 ± 0.05	4.11 ± 0.12
OG-3	20	2×10^{14}	1.4×10^6	5.0	1333.00 ± 0.03	3.50 ± 0.08
OG-4	20	2×10^{14}	3.5×10^6	12.5	1333.20 ± 0.04	4.43 ± 0.12

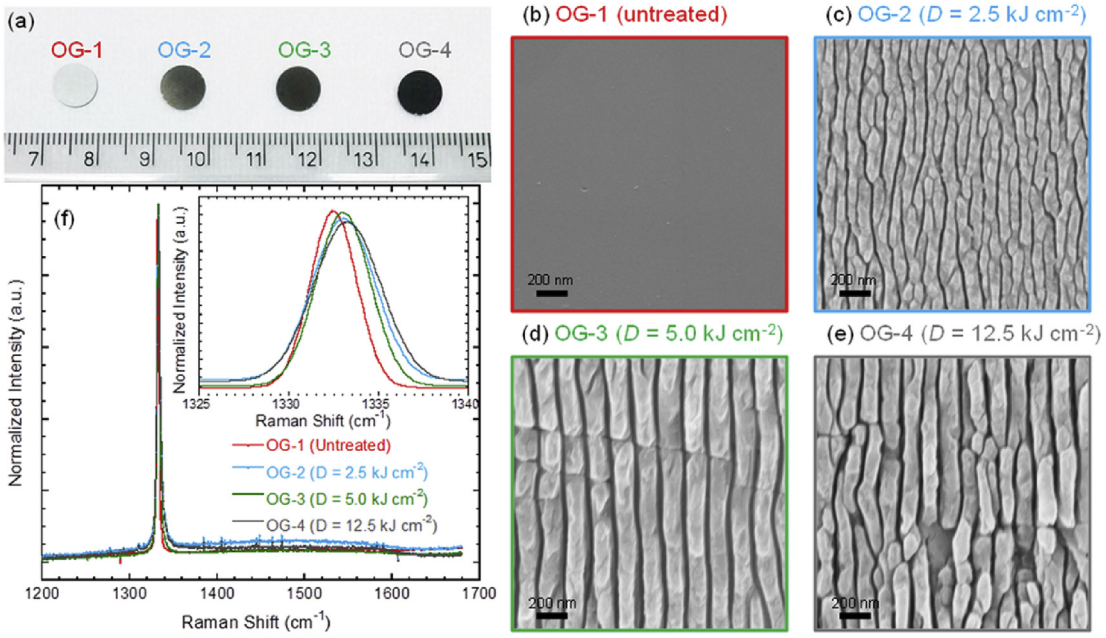

Fig. 1. (a) CVD Diamond samples used for the experiment reported in this paper, where the treatment dose increases from left (untreated) to right (12.5 kJ cm^{-2}). SEM images of CVD diamond surface correspond to: (b) surface-lapped pristine OG1; (c) OG-2 treated with a dose of 2.5 kJ cm^{-2}: a not well defined structure is formed without a regular periodicity; (d) OG-3 treated with a dose of 5.0 kJ cm^{-2}: a defined structure with a 170 nm periodicity is found; (e) OG-4 treated with a dose of 12.5 kJ cm^{-2}: formation of ripples is not homogeneous and grooves are sharply interrupted. (f) Comparison of Raman spectra for all investigated diamond samples. Diamond peaks are clearly defined around 1332 cm^{-1} and sp^2 phases are absent. Inset: zoom of the diamond Raman peaks in which it is possible to appreciate shifts and widths. (A colour version of this figure can be viewed online.)

2.2. Optical characterization

Optical absorption increase of fs-laser-textured samples was previously demonstrated and analyzed by the authors on lower quality CVD diamond samples [12,24]. Fig. 2 compares the absorptance spectra $A(\lambda)$ of optical-grade CVD diamond films treated at different doses, revealing a drastic increase of $A(\lambda)$ after the surface texturing according to an increasing function of D. It is useful to introduce the solar absorptance A_{solar}, defined as the integral of the product of $A(\lambda)$ and $W_{solar}(\lambda)$ (the global-tilt GT 1.5 air mass AM [30] solar irradiance) normalized to the integral of $W_{solar}(\lambda)$. A_{solar} estimates the radiation power absorbed by the samples: its dependence on treatment dose is shown in the inset of Fig. 2, where a phenomenological trend to saturation is evident. The obtained A_{solar} values are absolutely significant and competitive with commercial solar thermal absorbers [31]: 81.6% and 91.9% for sample treated at 5.0 kJ cm^{-2} and 12.5 kJ cm^{-2}, respectively.

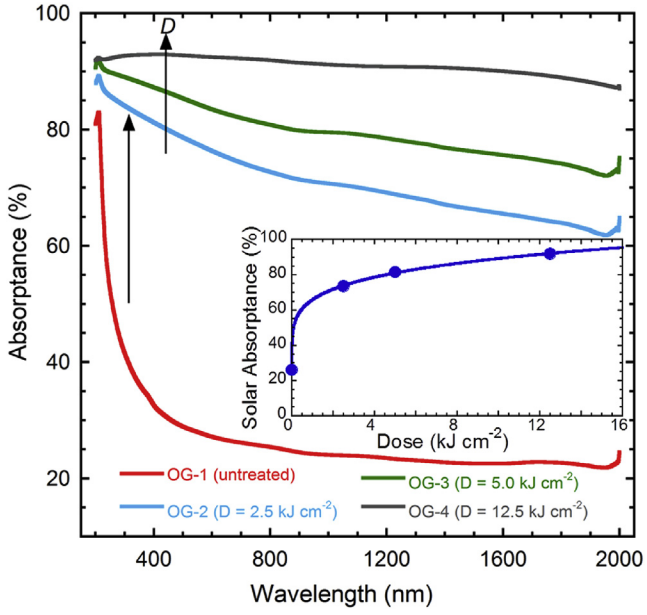

Fig. 2. Absorptance spectra of the samples. The surface texturing induces a significant absorption increase, that is an increasing function of the treatment dose D. The inset reports the solar absorptance of the samples as a function of surface treatment dose. The continuous line is reported for visual aid. (A colour version of this figure can be viewed online.)

2.3. Photoelectronic characterization

For an efficient solar device, absorbed photons have to generate useful charge carriers in the semiconductor, capable to move adequately in the active volume to contribute to the electric signal and/or to the energy conversion. For wide bandgap semiconductors like diamond, it means that defect energy levels have to be produced within the bandgap, namely an intermediate band, able to promote charge carriers generated by sub-bandgap photons into the extended bands. On the other hand, generated charges may experience interactions during the transport with the introduced defects. Consequently, necessary condition for the nature of the introduced defects is that they have to act as fast traps, characterized by short re-emission times, so that, in case of a scattering with the photocarriers, capturing is followed by a charge release after a suitably short time. Conversely, if defect states act as recombination centers, photocarriers are captured for long times, making their electrical contribution useless or even detrimental. Finally, the produced defects should be spatially localized in a small active region to favor the interaction with the impinging photons but not to perturb the material transport capabilities. To demonstrate that the described conditions can be satisfied by surface texturing, bulk photoconductivity spectra are derived by measuring the

photocurrent I_{ph} dependence on impinging monochromatic radiation wavelength λ. Such a characterization has been carried out by means of a Newport 74125 monochromator coupled to a xenon lamp, allowing operations in a wavelength range from 190 to 1100 nm. Monochromatic beam passed through a collimating and focusing lens system, and to a SR540 Chopper (14–733 Hz) before impinging on the sample. Samples were biased by means of a Keithley 487 electrometer and the photogenerated signal (modulus and phase) was collected by an EG&G Princeton Applied Research 5209 lock-in amplifier. For this characterization step, ohmic contacts have been fabricated on front and back surface ("sandwich" configuration) of diamond plates and wire bonded to a printed circuit board for applying the bias voltage V_b and extracting the photo-generated current I_{ph}. Front contact consists of two planar electrodes (2.0×6.0 mm^2, short circuited by wire bonding) separated by a distance of 1.0 mm, exactly equal to the spot-size of the focused impinging radiation beam: A schematic sketch of the measurement setup is shown in the inset of Fig. 3a. Responsivity $R(\lambda)$ of investigated samples is obtained as the ratio of I_{ph} to incident lamp power density for each wavelength, and quantum external efficiency $QE(h\nu)=(R \times h\nu)/q$, where q is the elementary charge and $h\nu$ is the photon energy. Fig. 3a shows the comparison of normalized responsivities for surface-textured and pristine samples with an applied electric field $F = 1$ V μm^{-1} and a modulation frequency of 14 Hz (i.e. low frequency to probe a response close to continuous wave excitation), whereas in Fig. 3b the normalized QE is reported as a function of $h\nu$. $R(\lambda)$ of the untreated sample shows a sharp peak at diamond bandgap (227 nm, $h\nu = 5.47$ eV) and an approximately flat response for sub-bandgap photon energies, decreasing for wavelengths longer than 600 nm.

The discrimination in responsivity between over- and sub-bandgap photon energies is larger than two orders of magnitude, lower than single-crystal diamond [2] but indicative of a low defect-density crystal. An increasing trend of $QE(h\nu)$ for the lowest photon energies saturates around 2.1 eV until $h\nu$ reaches the value of 4.5 eV, where an increase preludes the sharp response of diamond bandgap. Conversely, the surface textured samples show peculiar trends, depending on the treatment dose:

- At low doses ($D = 2.5$ kJ cm^{-2}), $R(\lambda)$ almost retraces the one of the untreated sample, inducing only an small enhancement in the 300–400 nm range;
- At medium doses ($D = 5.0$ kJ cm^{-2}), responsivity is significantly higher than the untreated sample for all the wavelength range, with an increase of two orders of magnitude in the 250–450 nm range. Such an increase reduces at higher wavelengths, before assuming similar values to the untreated case for $\lambda > 800$ nm. This finding suggests that surface texturing effectively contributes to electronically active defect states in a well-defined energy range. Responsivity enhancement is observable also for over bandgap photon energies, probably due to an increased geometric light trapping and to the combination of an optical coupling effect, being the texturing periodicity close to the corresponding radiation wavelength.
- At higher doses ($D = 12.5$ kJ cm^{-2}), unlike what expected from the optical characterization, responsivity drastically reduces. The nature of the introduced defects can be supposed to undergo a change from electrically active traps to recombination centers. If a significant amount of recombination centers is introduced and/or photocarriers experience a far lower capability of moving within the crystal, the resulting photocurrent is negatively affected, despite the enhancement of photon absorption.

3. Discussion

From reported characterizations, it clearly appears that surface texturing significantly enhances the optical absorption as well as it modifies the density of states within diamond bandgap. In order to investigate the correlation of the optical and electronic contributions and disentangle native defects within the crystal from the ones introduced by the surface texturing, we define:

$$k_{opt}(\lambda) = \frac{A_{textured}(\lambda)}{A_{untreated}(\lambda)}; \quad k_{pe}(\lambda) = \frac{QE_{textured}(\lambda)}{QE_{untreated}(\lambda)}, \tag{1}$$

being k_{opt} the optical absorptance gain and k_{pe} the photoelectronic gain, both referred to the respective parameters of the untreated material. In this way, the surface texturing contribution can be sharply discussed. The $k_{opt}(\lambda)$ and $k_{pe}(\lambda)$ trends for different

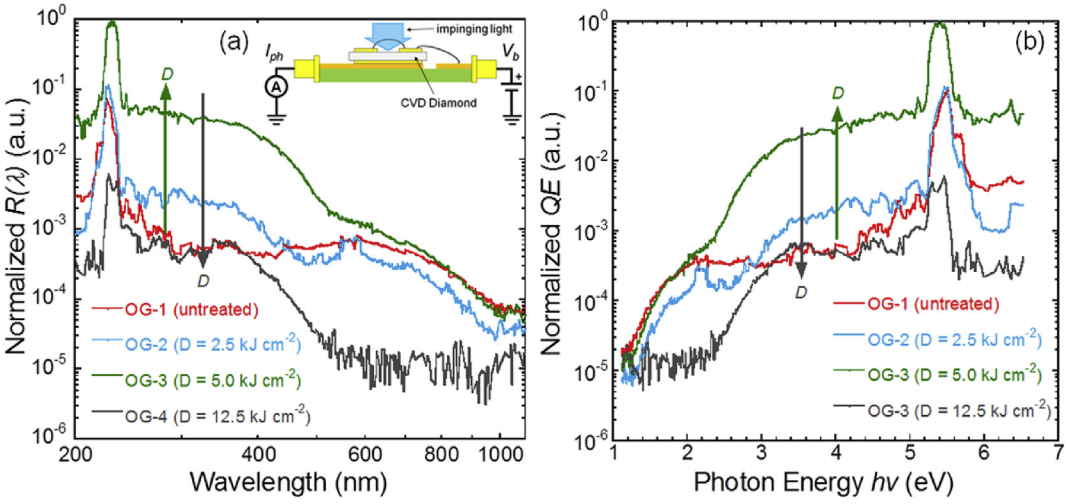

Fig. 3. (a) Normalized responsivity of investigated samples in the 190–1100 nm wavelength range, obtained as the ratio of photocurrent density to lamp power density. The applied electric field is 1 V μm^{-1} and the modulation frequency f is 14 Hz; it is possible to notice the enhancement due to laser treatment on OG-3 sample (green line), textured according to a medium value of dose of 5.0 kJ/cm^2. In the inset, a sketch of the measurement setup is shown, where the ammeter symbol resumes the measurement lock-in amplifier chain. (b) The resulting quantum efficiency as a function of photon energy for analyzed specimens. (A colour version of this figure can be viewed online.)

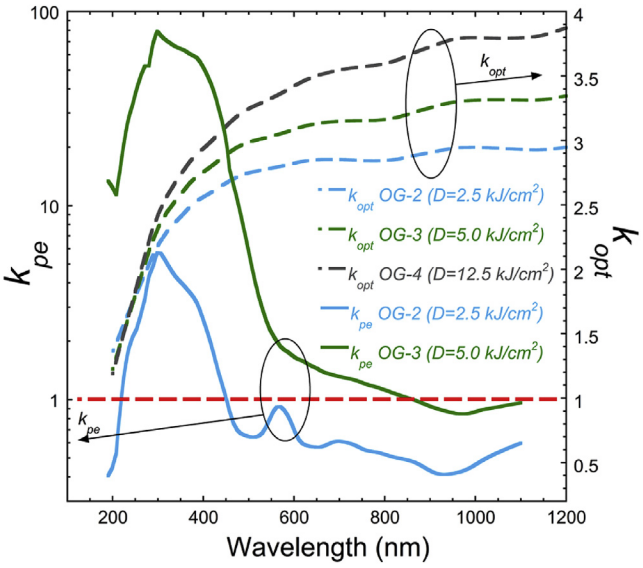

Fig. 4. Comparison between the photoelectronic k_{pe} (logarithmic scale) and optical k_{opt} (linear scale) gains measured for the surface-textured samples as a function of radiation wavelength. The red dashed line indicates the $k_{opt}(\lambda)$, $k_{pe}(\lambda) = 1$ condition (i.e. invariance with respect to the pristine diamond sample). (A colour version of this figure can be viewed online.)

treatment doses are reported in Fig. 4, where a red dashed line corresponds to k_{opt}, $k_{pe} = 1$: values over the line represent an increase of absorptance and photocurrent due to the texturing. The gains dependence on λ are significantly dissimilar, meaning that the close correlation between absorption coefficient and quantum efficiency [32] is not effective for black diamond. For wavelength close to diamond bandgap $k_{opt}(\lambda) \cong 1$, then it increases rapidly up to 600 nm to saturate at a constant value in the IR range (from 2.7 to 4.0 as a function of the treatment dose). Conversely, $k_{pe}(\lambda)$ appears as a broad peak ranging from 200 to 500 nm (2.5–6.0 eV), probably resulting from the linear combination of several local bands. When $D = 5.0$ kJ cm^{-2}, $k_{pe}(\lambda)$ shows a huge enhancement, equal to about 100 for $\lambda = 300$ nm and >1 up to 850 nm. For $D = 2.5$ kJ cm^{-2}, $k_{pe}(\lambda)$ reaches values around 10, after showing values < 1 for $\lambda > 450$ nm. The highest dose sample ($D = 12.5$ kJ cm^{-2}) has a $k_{pe}(\lambda) < 1$ in all the explored range, not reported in Fig. 4.

The physical meaning of $k_{pe}(\lambda)$ can be exclusively explained with an increase of defect states introduced in the crystal by the surface-texturing which generate electron–hole couples and do not affect with their transport within the crystal. In particular, sample treated at $D = 5.0$ kJ cm^{-2} shows a k_{pe} ranging from 2 to 1 for $\lambda > 550$ nm, where k_{opt} is around 3: photons with these wavelengths are absorbed by the crystal but they do not produce photocarriers because 1) no defect states with proper energy levels have been created or 2) the photogenerated carriers are immediately captured by these defect levels (i.e. recombination centers). In both cases, no production of useful charges occurs. For $\lambda < 550$ nm, $k_{pe} >> k_{opt}$: consequently, the increased absorption capability cannot justify the stronger enhancement of photogenerated carriers. Surface texturing acts in a twofold independent way: optically it is able to efficiently capture visible and IR radiation and, at the same time, it adds electrically-active defect levels which form a band within diamond bandgap, able to interact with photons in the 2.5–5.5 eV energy range, classifiable as an intermediate band [33]. It is worth to notice that modulated photoconductivity technique does not allow discrimination between electrons and holes because photocurrent results from the joint density of states [34], thus the absolute position within the bandgap of the intermediate band cannot presently be determined.

To better analyze the photoelectronic behavior, it is interesting to quantify the effect of the surface texturing on transport properties of diamond films. The most important figure-of-merit for the sensitivity of a photoconductor is the mobility-lifetime product $\mu\tau$, estimated from $I_{ph}(V_b)$ characteristics, being V_b the applied bias, when the samples are impinged by an over-bandgap radiation (e.g. $\lambda = 225$ nm). In this case, the radiation penetration length is some micrometers under the diamond surface, where the charge carriers are produced. For diamond, $I_{ph}(V_b)$ is well described by Hecht's equation [35]:

$$I_{ph} = qG_0\Lambda\,\frac{\mu\tau V_b}{d}\left[1 - \exp\left(-\frac{d^2}{\mu\tau V_b}\right)\right], \qquad (2)$$

where G_0 is the generation rate (the volume concentration of generated carriers per unit time), d is the sample thickness, and Λ is the illuminated area. Hecht's equation considers that I_{ph} saturates at an electric field where the collection distance $\mu\tau F$ is larger than the distance travelled by both the charge carriers (the sample thickness, in our case). The saturation corresponds to the collection of the maximum amount of available photocarriers. Equation (2) is used to fit the experimental data reported in Fig. 5 to obtain the $\mu\tau$ product, that is an average value between $\mu\tau$ of electrons and holes. The untreated diamond sample shows a best-fitted $\mu\tau = 1.4 \times 10^{-5}$ cm^2 V^{-1}, the reference value to be compared with black diamond ones. For the discussion, we assume that average mobility μ is a constant for all the investigated samples, so that lifetime τ is the electronic property influenced by laser treatment. This arbitrary hypothesis considers that the carrier transport occurs prevalently within the diamond bulk, which has been demonstrated by Raman spectroscopy not to be structurally affected by the texturing. On the other hand, τ can experience significant modifications at the textured surface, where defect levels are introduced and photocarriers are generated.

The sample textured at $D = 2.5$ kJ cm^{-2} shows photocurrent similar to the untreated one, but smaller $\mu\tau$ due to the starting of saturation regime at a higher V_b, reasonably induced by deeper levels within the bandgap, affecting carriers lifetime. Conversely,

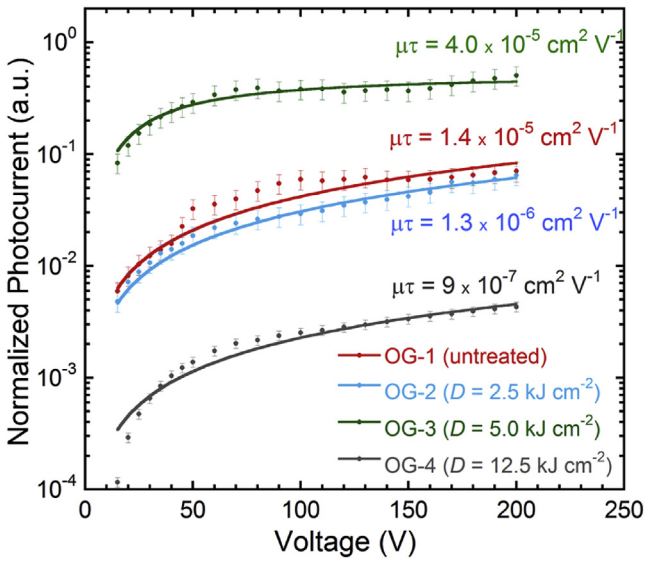

Fig. 5. Normalized photocurrent characteristics measured on all the samples by irradiating them with an over-bandgap monochromatic 225 nm radiation beam modulated at a frequency of 14 Hz. Experimental data are well fitted by the Hecht formula reported in Equation (2). (A colour version of this figure can be viewed online.)

the sample textured at medium dose shows a significant photocurrent increase as well as in $\mu\tau$, equal to 4.0×10^{-5} cm^2 V^{-1}. Here, surface texturing introduced defect levels sufficiently close to bandgap edge that, acting as traps for one charge carrier type, give rise to a trap-assisted transport, namely the so-called "sensitization mechanism" [36]. Recombination processes typically occur through band-to-band recombination or, if present, through recombination centers, where one carrier type first enters the center, after which the other carrier quickly recombines with it. In case of traps for one carrier type, also called "sensitizing centers", the trap cross-sections are significantly unbalanced. If, for example, trap cross-section is very small for the electron, the electron will be free for an extended period of time after the hole is trapped. For an extremely small cross section, the trapped carrier may be thermally excited back to the band, so that the overall carrier lifetime can terminate by band-to-band recombination. The lifetime depends on the time spent in the trap by the carrier, thus the introduction of sensitizing centers provides a mechanism for enhancing significantly the resulting lifetime and improving the photoconductivity. Finally, the sample treated at $D = 12.5$ kJ cm^{-2} shows the lowest photocurrent and $\mu\tau$ values, probably due to a high density of recombination centers probably originated by the reported surface damages.

It is worth considering the total charge generated within the black diamond if irradiated with solar light with respect to a possible energy conversion mechanism. Supposing that:

- all the photogenerated charge carriers can be transported from the generation zone to the electrodes by an internal field. This is possible with a proper band-bending produced by a specific semiconductor structure acting as an energy active device (for example the structure proposed in [37]);
- it is possible to exploit all the photocharges, whose value can be considered as an upper limit for the energy conversion;
- black diamond technology is applied to a very low defect density diamond sample with a quantum efficiency equal to 1 at diamond bandgap;
- Surface texturing acts on the considered diamond plate by inducing the same $QE(h\nu)$ trend reported for the sample textured under the best conditions ($D = 5.0$ kJ cm^{-2});

it can be approximated an upper limit for the amount of photons converted into electric charge by black diamond semiconductor structure in interacting with the solar radiation spectrum. Defining the integrated solar quantum efficiency as:

$$QE_{solar} = \frac{\int_0^\infty QE(h\upsilon) \cdot W_{solar}(h\upsilon) d(h\upsilon)}{\int_0^\infty W_{solar}(h\upsilon) d(h\upsilon)}, \quad (3)$$

where, for the specific explored range, the lower and upper integration limits reduce to 1.13 and 6.53 eV, respectively. QE_{solar} estimates the amount of photons in the solar spectrum converted into charge carriers. Equation (3) applied to the experimental data gives $QE_{solar} = 0.54\%$, that has to be considered the first quantitative evaluation in the diamond defect engineering strategy. Indeed, the introduced intermediate band has to be increased in terms of density and, above all, in terms of energy matching with the solar spectrum.

In any case, the most immediate application of black diamond, especially in its high-defect-density but large-area low-cost polycrystalline form, is as a competitive high-temperature radiation absorber for solar thermodynamic conversion, due to a solar absorptance larger than 90% and high thermal resistance. A future higher added value application can be as photo-thermionic cathode for PETE devices. In this case, the advantage derives from the low work function values achievable with diamond and the high solar absorption capability causing high temperature operations. The temperature increase induces thermionic emission, that can be coupled to the discussed photoelectronic boost, directly derived from the conversion of photons into hot carriers. Hot electrons able to reach the surface, thermalize and contribute to the emission. In other words, every thermalization process contributes to thermionic emission, whereas direct photogeneration, increasing extremely the electron population at the conduction band above the equilibrium level, further reduces the emission energy barrier, thus allowing very high conversion efficiencies [38].

4. Conclusions

CVD diamond samples were surface-textured by means of a femtosecond laser beam to provide and optimize a new material: black diamond, whose properties are tailored to optically and electrically interact with solar radiation. Surface texturing by fs-laser represents a technologically easy process to fabricate ripples with a periodicity of about 170 nm on diamond. Solar absorptance larger than 90% demonstrated the treatment optical efficacy. The process is also a useful tool for implementing a defect-engineering on the electronic properties of diamond, that induces the formation of an intermediate band. The present photoelectronic performance with respect to solar radiation conversion represents the first step towards an enhanced defect engineering strategy that is going to be optimized by acting on an improved control of the process parameters (e.g. by developing a 2D periodic surface structure, reducing the periodicity, controlling the depth, structure shape, etc.).

Supplementary video related to this article can be found at http://dx.doi.org/10.1016/j.carbon.2016.04.017.

Acknowledgements

The activity was supported by the European Community FP7-Energy Project ProME^{3}ThE^{2}US^2 "*Production Method of Electrical Energy by Enhanced Thermal Electron Emission by the Use of Superior Semiconductors*", Grant Agreement n. 308975, website: www.prometheus-energy.eu.

References

[1] R.S. Balmer, J.R. Brandon, S.L. Clewes, H.K. Dhillon, J.M. Dodson, I. Friel, et al., Chemical vapour deposition synthetic diamond: materials, technology and applications, J. Phys. Condens. Matter. 21 (2009) 364221.
[2] D.M. Trucchi, P. Allegrini, P. Calvani, A. Galbiati, K. Oliver, G. Conte, Very Fast and primingless single-crystal-diamond X-ray dosimeters, IEEE Electron Device Lett. 33 (2012) 615–617.
[3] M. Pomorski, B. Caylar, P. Bergonzo, Super-thin single crystal diamond membrane radiation detectors, Appl. Phys. Lett. 103 (2013) 112106.
[4] M. Marinelli, E. Milani, G. Prestopino, M. Scoccia, A. Tucciarone, G. Verona-Rinati, et al., High performance ^{6}LiF-diamond thermal neutron detectors, Appl. Phys. Lett. 89 (2006) 143509.
[5] A. Bellucci, S. Orlando, D. Caputo, E. Cappelli, D.M. Trucchi, Dosimetric performance of single-crystal diamond X-Ray Schottky photodiodes, IEEE Electron Device Lett. 34 (2013) 695–697.
[6] M. Girolami, A. Bellucci, P. Calvani, C. Cazzaniga, M. Rebai, D. Rigamonti, et al., Mosaic diamond detectors for fast neutrons and large ionizing radiation fields, Phys. Status Solidi 212 (2015) 2424–2430.
[7] K. Ueda, M. Kasu, Y. Yamauchi, T. Makimoto, M. Schwitters, D. Twitchen, et al., Diamond FET using high-quality polycrystalline diamond with fT of 45 GHz and fmax of 120 GHz, Electron Device Lett. IEEE 27 (2006) 570–572.
[8] P. Calvani, A. Corsaro, M. Girolami, F. Sinisi, D.M. Trucchi, M.C. Rossi, et al., DC and RF performance of surface channel MESFETs on H-terminated polycrystalline diamond, Diam. Relat. Mater. 18 (2009) 786–788.
[9] T. Sun, F.A.M. Koeck, A. Rezikyan, M.M.J. Treacy, R.J. Nemanich, Thermally enhanced photoinduced electron emission from nitrogen-doped diamond films on silicon substrates, Phys. Rev. B 90 (2014) 121302.

[10] A. Bellucci, P. Calvani, E. Cappelli, S. Orlando, D. Sciti, R. Yogev, A. Kribus, D.M. Trucchi, Preliminary characterization of ST2G: solar thermionic-thermoelectric generator for concentrating systems, AIP Conf. Proc. 1667 (2015) 020007. ISSN: 0094243X.
[11] J.W. Schwede, I. Bargatin, D.C. Riley, B.E. Hardin, S.J. Rosenthal, Y. Sun, et al., Photon-enhanced thermionic emission for solar concentrator systems, Nat. Mater 9 (2010) 762–767.
[12] P. Calvani, A. Bellucci, M. Girolami, S. Orlando, V. Valentini, A. Lettino, et al., Optical properties of femtosecond laser-treated diamond, Appl. Phys. A Mater. Sci. Process 117 (2014) 25–29.
[13] G. Dumitru, V. Romano, H.P. Weber, M. Sentis, W. Marine, Femtosecond ablation of ultrahard materials, Appl. Phys. A Mater. Sci. Process 74 (2002) 729–739, http://dx.doi.org/10.1007/s003390101183.
[14] M. Girolami, A. Bellucci, P. Calvani, S. Orlando, V. Valentini, D.M. Trucchi, Raman investigation of femtosecond laser-induced graphitic columns in single-crystal diamond, Appl. Phys. A 117 (2014) 143.
[15] Q. Wu, Y. Ma, R. Fang, Y. Liao, Q. Yu, X. Chen, et al., Femtosecond laser-induced periodic surface structure on diamond film, Appl. Phys. Lett. 82 (2003) 1703.
[16] P.P. Rajeev, M. Gertsvolf, C. Hnatovsky, E. Simova, R.S. Taylor, P.B. Corkum, et al., Transient nanoplasmonics inside dielectrics, J. Phys. B At. Mol. Opt. Phys. 40 (2007) S273–S282.
[17] B. Stuart, M. Feit, A. Rubenchik, Laser-induced damage in dielectrics with nanosecond to subpicosecond pulses, Phys. Rev. Lett. 74 (1995) 2248–2252.
[18] T.J.-Y. Derrien, T.E. Itina, R. Torres, T. Sarnet, M. Sentis, Possible surface plasmon polariton excitation under femtosecond laser irradiation of silicon, J. Appl. Phys. 114 (2013) 083104.
[19] J.Z.P. Skolski, G.R.B.E. Römer, J.V. Obona, V. Ocelik, A.J. Huis in 't Veld, J.T.M. De Hosson, Laser-induced periodic surface structures: fingerprints of light localization, Phys. Rev. B 85 (2012) 075320.
[20] Z. Yin, Z. Akkerman, B. Yang, F. Smith, R.E. Ted, Optical properties and microstructure of CVD diamond films, Diam. Relat. Mater 6 (1997) 153–158.
[21] P.K. Bachmann, H.D. Bausen, H. Lade, D. Leers, D.U. Wiechert, N. Herres, et al., Raman and X-ray studies of polycrystalline CVD diamond films, Diam. Relat. Mater 3 (1994) 1308–1314.
[22] C. Casiraghi, A. Ferrari, J. Robertson, Raman spectroscopy of hydrogenated amorphous carbons, Phys. Rev. B 72 (2005) 085401.
[23] C. Pickard, T. Davis, W. Wang, J. Steeds, Mapping crystalline quality in diamond films by micro-Raman spectroscopy, Diam. Relat. Mater. (1998) 238–242.
[24] P. Calvani, A. Bellucci, M. Girolami, S. Orlando, V. Valentini, R. Polini, et al., Absorptance enhancement in fs-laser-treated CVD diamond, Phys. Status Solidi 212 (2015) 2463–2467.
[25] P. Calvani, A. Bellucci, M. Girolami, S. Orlando, V. Valentini, R. Polini, et al., Infrared absorption of fs-laser textured CVD Diamond, Appl. Phys. A Mater. Sci. Process 122 (2016) 211.
[26] E.J. Di Liscia, Stress analysis on single-crystal diamonds by Raman spectroscopy 3D mapping, Mater. Sci. Appl. 04 (2013) 191–197.
[27] A. Haouni, M. Mermoux, B. Marcus, L. Abello, G. Lucazeau, Confocal Raman imaging for the analysis of CVD diamond films, Diam. Relat. Mater 8 (1999) 657–662.
[28] S. Prawer, R.J. Nemanich, Raman spectroscopy of diamond and doped diamond, Philos. Trans. A. Math. Phys. Eng. Sci. 362 (2004) 2537–2565.
[29] Z. Sun, J.R. Shi, B.K. Tay, S.P. Lau, UV Raman characteristics of nanocrystalline diamond films with different grain size, Diam. Relat. Mater 9 (2000) 1979–1983.
[30] R.E. Bird, R.L. Hulstrom, L.J. Lewis, Terrestrial solar spectral data sets, Sol. Energy 30 (1983) 563–573.
[31] M. Romero, A. Steinfeld, Concentrating solar thermal power and thermochemical fuels, Energy Environ. Sci. 5 (2012) 9234.
[32] R.H. Bube, Photoelectronic Properties of Semiconductors, Cambridge University Press, Cambridge, United Kingdom, 1992.
[33] A. Luque, A. Martí, C. Stanley, Understanding intermediate-band solar cells, Nat. Photonics 6 (2012) 146–152.
[34] H. Oheda, Phase-shift analysis of modulated photocurrent: its application to the determination of the energetic distribution of gap states, J. Appl. Phys. 52 (1981) 6693–6700.
[35] K. Hecht, Zum Mechanismus des lichtelektrischen Primarstromes in isolierenden Kristallen, Z. Für Phys. 77 (1932) 235–245.
[36] A. Rose, Concepts in Photoconductivity and Allied Problems, Krieger Publishing Co., Huntington, New York, USA, 1978.
[37] A. Bellucci, P. Calvani, M. Girolami, D.M. Trucchi, Defect engineering of diamond cathodes for high temperature solar cells, in: Proc. 15th IEEE Int. Conf. Environ. Electr. Eng., 2015, pp. 1616–1619.
[38] G. Segev, Y. Rosenwaks, A. Kribus, Limit of efficiency for photon-enhanced thermionic emission vs. photovoltaic and thermal conversion, Sol. Energy Mater. Sol. Cells 140 (2015) 464–476.